HHS Public Access

Author manuscript

Technol Cancer Res Treat. Author manuscript; available in PMC 2015 May 14.

Published in final edited form as:

Technol Cancer Res Treat. 2013 August ; 12(4): 311–321. doi:10.7785/tcrt.2012.500321.

A Comparative Evaluation of Ultrasound Molecular imaging, Perfusion Imaging, and Volume Measurements in Evaluating Response to Therapy in Patient-Derived Xenografts

J.E. Streeter, MS[1], **S.G. Herrera-Loeza, BS**[2], **N.F. Neel, PhD**[2,3], **J.J. Yeh, MD**[2,3,4], and **P.A. Dayton, PhD**[1,2,*]

[1]Joint Dept. of Biomedical Engineering, University of North Carolina-North Carolina State University, Chapel Hill, NC, USA

[2]Lineberger Comprehensive Cancer Center, University of North Carolina, Chapel Hill, NC, USA

[3]Department of Pharmacology, University of North Carolina, Chapel Hill, NC, USA

[4]Department of Surgery, Division of Surgical Oncology, University of North Carolina, Chapel Hill, NC, USA

Abstract

Most pre-clinical therapy studies use the change in tumor volume as a measure for disease response. However, tumor size measurements alone may not reflect early changes in tumor physiology that occur as a response to treatment. Ultrasonic molecular imaging (USMI) and Dynamic Contrast Enhanced - Perfusion Imaging (DCE-PI) with ultrasound are two attractive alternatives to tumor volume measurements. Since these techniques can provide information prior to the appearance of gross phenotypic changes, it has been proposed that USMI and DCE-PI could be used to characterize response to treatment earlier than traditional methods. This study evaluated the ability of tumor volume measurements, DCE-PI, and USMI to characterize response to therapy in two different types of patient-derived xenografts (known responders and known non-responders). For both responders and non-responders, 7 animals received a dose of 30 mg/kg of MLN8237, an investigational aurora-A kinase inhibitor, for 14 days or a vehicle control. Volumetric USMI (target integrin: $\alpha_v\beta_3$) and DCE-PI were performed on day 0, day 2, day 7, and day 14 in the same animals. For USMI, day 2 was the earliest point at which there was a statistical difference between the untreated and treated populations in the responder cohort (Untreated: 1.20±0.53 vs. Treated: 0.49±0.40; $p < 0.05$). In contrast, statistically significant differences between the untreated and treated populations as detected using DCE-PI were not observed until day 14 (Untreated: 0.94±0.23 vs. Treated: 1.31±0.22; $p < 0.05$). Volume measurements alone suggested no statistical differences between treated and untreated populations at any readpoint. Monitoring volumetric changes is the “gold standard” for evaluating treatment in pre-clinical

[*]**Corresponding Author:** Paul A. Dayton, Address: 304 Taylor Hall, 109 Mason Farm Road, Chapel Hill, NC, 27599-6136, Phone: (919) 843-9521 Fax: (919) 843-9520, padayton@bme.unc.edu.

Conflict of Interest

This work is original and has not been accepted for publication in any other peer-reviewed journal. Dr. Paul Dayton is on the Scientific Advisory Board for Targeson, Inc.

studies, however, our data suggests that volumetric USMI and DCE-PI may be used to earlier classify and robustly characterize tumor response.

Keywords

Ultrasound; 3-D; Microbubbles; Molecular Imaging; Perfusion Imaging; Response to Therapy

Abbreviations

MCA; USMI; DCE-PI; CPS; 3-D; 2-D; MVD; PDX

Introduction

Aurora-A Kinase Inhibition

Aurora kinase, a type of serine/threonine kinase, is part of a family of enzymes related to cell proliferation (1). In the mid 1990's, it was discovered that aurora kinase defects led to mitotic abnormalities (2). Disruption of the functional process involving aurora kinase can result in mitotic spindle apparatus deficiencies, chromosome segregation abnormalities and eventually apoptosis (3). The discovery that aurora kinases are highly expressed in many tumor cell lines, including pancreatic adenocarcinoma (4), has led to the development of a variety of aurora kinase inhibitors, such as MLN8237, for tumor research (5, 6, 7). MLN8237, an orally administered aurora-A kinase inhibitor is currently in clinical trials for patients with advanced solid tumors; emerging data suggests that it may be active in some adult solid tumors (8)(9).

Response to therapy

Anatomic measures of solid tumors have been the "gold standard" by which therapy effectiveness is evaluated (10). The disadvantage to using size measurements to analyze response is that although the tumor volume may not have changed significantly, there may be considerable changes in tumor activity and necrosis (11, 12). In many instances, there may be a significant delay or lag time between the time of treatment and any change in tumor size (10). Thus, new early imaging response techniques are sought after to non-invasively predict treatment response both clinically and pre-clinically. Ultrasonic molecular imaging (USMI) and Dynamic Contrast Enhanced - Perfusion Imaging (DCE-PI) are two attractive alternatives.

Ultrasonic Molecular Imaging

USMI has the ability to non-invasively characterize biologic processes at the cellular and molecular level (13, 14, 15). The principle behind USMI is the selective targeting of acoustically active intravascular microbubble contrast agents (MCAs) to biomarkers expressed on the endothelium (16). Once accumulated at the target site, the MCAs enhance the acoustic backscatter from pathologic tissue that might otherwise be difficult to distinguish from normal tissues. While USMI is still a developing field, a wide variety of techniques are emerging such as assessment of tumor angiogenesis, the diagnosis of

myocarditis, the evaluation of transplant rejection, the evaluation of cardiovascular disease, and the imaging of dysfunctional endothelium, and thrombus (17, 14, 18, 19).

MCAs are inherently blood pool agents, thus USMI is restricted to analysis of biological events located within the vascular system. This particular characteristic makes this imaging modality an attractive non-invasive technique for the detection of molecular processes on vascular endothelial cells, and more specifically, tumor angiogenesis. Tumor angiogenesis is the formation of capillaries and new blood vessels from surrounding host tissue to provide sufficient oxygen supply and nutrients to the tumor (20). As cancer cells proliferate, more oxygen and nutrients are needed for cell survival. Thus, at the onset of hypoxia after cell proliferation, tumors will assemble vasculature by releasing chemotactic signals to recruit endothelial precursor cells (20). Presumably, any impairment of tumor growth and apoptosis has a downstream effect on angiogenesis and therefore angiogenic integrins (VEGFR-2, $\alpha_v\beta_3$, etc.) expressed on endothelial cells in proximity to the tumor (21, 22).

In recent years, targeted agents have been successfully used for non-invasive two-dimensional in vivo imaging of tumor angiogenesis (23, 24, 25, 26, 27), and more recently USMI has been demonstrated in 3-D (28, 29). This breakthrough has allowed USMI to be used for quantifying the efficacy of anti-angiogenic drugs such as bevacizumab (VEGF inhibitor) in murine models (26, 30, 31).

Dynamic Contrast Enhanced - Perfusion Imaging

Ultrasound DCE-PI is a method that is used to non-invasively monitor the blood flow in both large vessels and in the capillary microcirculation using non-targeted MCAs. This technique uses a short high-intensity pulse of ultrasound that causes rapid destruction of MCAs in the interrogated region. This clearance pulse is immediately followed by a low-intensity contrast specific signal that does not fracture the microbubbles, but instead, allows for the pixel-by-pixel observation of blood flow rates as the MCAs enter back into the tissue (32, 33). Accordingly, changes in contrast enhancement over time can provide information about tissue perfusion. This method has previously been utilized to assess perfusion in the myocardium, kidney, and other tissues (33, 34, 32). Furthermore, it is hypothesized that tissue perfusion correlates to tumor micro vessel density (MVD) (35, 36), a known prognostic factor in many cancer types (37, 38), which has been the motivation for the development of this technique in cancer assessment. Thus, it is proposed that in vivo measures using DCE-PI may also predict therapeutic response to agents that target and disrupt the tumor microvasculature.

It is unknown as to what method provides the best opportunity for successful pre-clinical evaluations, though our hypothesis predicts that USMI will provide information earlier in the treatment schedule than both DCE-PI and volume measurements. A recent study by Sirsi et al, which aimed to evaluate both molecular imaging and perfusion imaging in a response to therapy study (VEGF Inhibition in SK-NEP-1 tumor line), supports our hypothesis (39). Although this study was performed only with 2-D ultrasound, it was highly significant in suggesting the potential of DCE-PI and USMI in the evaluation of a tumor's response to therapy. As recent studies have illustrated that 3-D ultrasound DCE-PI and 3-D USMI provide more accurate data regarding tissue blood flow and biomarker distribution than 2-D

ultrasound, it is crucial to validate these technologies with volumetric imaging (28, 40, 41). Thus, the aim of this study is to further validate the potential of USMI and DCE-PI in characterizing a tumor's response to therapy using 3-D ultrasound.

To test our hypothesis, we use USMI of angiogenesis and DCE-PI, both implemented in 3-D, to evaluate the effect of MLN8237 in patient-derived xenografts (PDX) of pancreatic cancer. PDX models of solid tumors have recently emerged as an innovative platform for the study of novel therapeutics for pancreatic cancer (42). This model, where actual human tumors are grafted into mice, has been shown to be a better predictor of response to therapies in patients compared to traditional cell line xenografts (43). We use a Siemens Sequoia ultrasound system (Mountain View, CA) in Cadence Pulse Sequencing (CPS) mode for both perfusion and molecular imaging studies. In addition, with the use of a custom computer-controlled motion stage interfaced to the ultrasound system, we perform volumetric imaging by scanning the transducer elevationally at controlled intervals for a more robust evaluation of therapy effectiveness (40, 28). Finally, we compare and elucidate the strength of each technique as a tool to classify responders and non-responders and to characterize how a tumor will respond to therapy over time in our PDX models.

Materials and Methods

Microbubble Contrast Agents (MCAs)

MCAs designed to target $\alpha_v\beta_3$ integrins were created with a 9:0.5:0.5 molar ratio of 1,2 Distearoyl- sn-Glycero-3-Phosphocholine (DSPC) (Avanti Polar Lipids - Alabaster, AL), 1,2-Distearoyl-sn-Glycero-3-Phosphoethanolmine-N–Methoxy-Polyethylene Glycol-2000 (DSPE-PEG2000) (Avanti Polar Lipids – Alabaster, AL), and DSPE-PEG2000 cross-linked to a cyclic RGD peptide (Cyclo-Arg-Ala-Asp-D-Tyr-Cys) (Peptides International - Louisville, KY) as previously described (29). The chosen cyclic RGD peptide has previously been shown to target $\alpha_v\beta_3$-expressing vasculature, which is characteristic of angiogenic tumors (44, 29, 28). MCAs with a large preferentially selected mean diameter (~3.9 μm) have been shown to produce greater backscatter intensities in molecular imaging studies as compared to vial-shaken unsorted polydisperse distributions (29, 45); therefore, all MCAs in this study were size-selected via the method as presented by Feshitan and colleagues (46). Unsorted non-targeted MCAs for perfusion imaging were created with a similar lipid formulation, but without the targeting ligand.

Animal Preparation and Contrast Administration

Two PDXs were chosen for this study, one with known response to MLN8237 (PDX-R) and one with no response (PDX-NR) to MLN8237 based on tumor size measurements and long-term growth curves in previous studies. Each PDX (PDX-R and PDX-NR) was expanded into 14 nude mice (PDX-R & PDX-NR: Mean Volume ~ 0.2 ± 0.1 cm^3). Seven mice were then assigned to drug treatment or vehicle groups for both USMI and DCE-PI experiments. All animal studies were performed in accordance with protocols approved by the University of North Carolina School of Medicine Institutional Animal Care and Use Committee. During ultrasound imaging studies, animals were anesthetized with ~2% inhaled isoflurane anesthesia with oxygen and their body temperature was maintained at 37° C through the use

of a temperature-controlled heating pad. The area to be imaged was coupled to the ultrasound transducer using a water-based acoustic coupling gel devoid of any air bubbles. A 27-gauge catheter was inserted into the tail vein of the animal for the administration of MCAs. In all USMI experiments, bolus MCA injections of 50 μL (Concentration: 1×10^8 MCAs/mL) were delivered followed by an immediate flush of at least 50 μL sterile saline to clear any remaining MCAs from the catheter. For all DCE-PI experiments, non-targeted MCAs were continuously infused at a rate of 15 μL/min using a PHD-2000 syringe pump (Harvard Apparatus – Holliston, MA).

Therapy

A total of 28 nude mice (N=14 PDX-R and N=14 PDX-NR's) were used for USMI and DCE-PI experiments. Animals were either treated with 30 mg/kg of MLN8237 or a vehicle control daily by oral gavage over a 14-day period. For all experiments, USMI and DCE-PI data were taken on day 0, day 2, day 7, and day 14 during the treatment period in the same animals.

3-D Imaging Apparatus

A Siemens Sequoia imaging system (Acuson Sequoia 512 – Mountainview, CA) with a linear array transducer (Model # 15L8) was used to acquire all ultrasound images in both USMI and DCE-PI studies. To create 3-D data sets, the transducer was scanned elevationally using a linear motion stage (Model UTS150PP, Newport – Irvine, CA). A custom LabView (National Instruments – Austin, TX) program was interfaced to both the motion stage and the ultrasound system, enabling the control of step-sizes, and triggering the capture of video data at every discrete step as previously described by Feingold et al and Streeter et al (28, 40).

Ultrasonic Molecular Imaging

Cadence pulse sequencing (CPS) mode was used in all studies (USMI and DCE-PI). CPS is a non-destructive contrast-specific imaging mode developed by Siemens, which has been used for both perfusion and molecular imaging (47). Prior to imaging tumors with targeted contrast agents, background data was taken in both b-mode and CPS mode to optimize elevational scan length and to ensure the absence of bubbles within the coupling gel. After the initial background scans were performed, the system was paused and a 50 μL bolus injection of contrast agents was administered through the catheter followed by a 50 μL flush with sterile saline. After waiting approximately 15 minutes for freely-circulating bubbles to clear from the animal's system, a 3-D imaging scan was acquired across the tumor with inter-plane step sizes of 400 μm in the ultrasound system's CPS mode. The bound microbubbles were then destroyed using a high mechanical index b-mode volumetric scan, and then the tumor was re-imaged in CPS mode at the same slice locations for a baseline measurement with no targeted agents. Within each data set, the system receive gain (−15 dB), and transmit power (MI: 0.18) were kept constant and the axial focus was always positioned in the center of the tumor for each animal's readpoints. The time required for each molecular imaging study was approximately 30 minutes per animal.

Video data from targeting experiments were acquired and saved in compressed DICOM format for offline analysis. Using b-mode image data collected prior to contrast administration, ROIs were established around the perimeter of the tumor in each image plane. With custom MATLAB scripts, the difference in mean pixel intensity between the pre-destruction pulse image (the image with adherent MCAs) and the background image was determined for each image plane as a measure of $\alpha_v\beta_3$ targeting, similar to previous molecular imaging studies with ultrasound (29, 28).

Dynamic Contrast Enhanced - Perfusion Imaging

DCE-PI was performed by using the destruction-reperfusion imaging technique previously described by Wei et al (32) and real-time motion correction was performed as described by Pollard et al (34). The “CPS Capture” software tool was used to implement this technique. Briefly, non-targeted contrast agents were continuously infused at a rate of 15 μL/min. After a wait period of one minute for complete tumor perfusion, a contrast specific frame was collected and recorded by the system. Then, a short high-intensity pulse of ultrasound that causes rapid destruction of MCAs in the 2-D imaging plane was introduced. This clearance pulse was immediately followed by a low-intensity contrast specific interrogation to monitor the MCAs as they entered back into the tissue. When the monitored contrast signal reached 20% (Time to 20% - TT20) of the previously recorded image, the time was recorded and displayed as a color. Perfusion mapping occurred at the pixel level and the maximum perfusion time window was set to be 20 seconds for all readpoints. Within each data set, the system receive gain (−15 dB), and transmit power were kept constant. Perfusion imaging studies required approximately 10 minutes per animal.

Video data from perfusion imaging experiments were acquired and saved in compressed DICOM format for offline analysis. Using the b-mode image data collected during the MCA destruction sequence, ROIs were established around the perimeter of the tumor in each image plane. With custom MATLAB scripts, the mean pixel intensity, which is linearly related to the time that it takes to reach 20% of the pre-destructive value, was averaged for all voxels throughout the perfused volume of the treated tumor.

Volume Measurements

Volume measurements for each tumor were obtained using the b-mode images acquired during USMI experiments in conjunction with the elevational step size.

Statistical Analysis

For USMI experiments, the amount of microbubble targeting for the volume of the tumor was quantified as the difference between the mean pixel intensity within the user-defined volume with targeted microbubbles and the mean pixel intensity of the volume after the MCAs were destroyed. At each readpoint, the amount of microbubble targeting was normalized to the value obtained at baseline (day 0).

For DCE-PI experiments, the time that it takes to reach 20% of the pre-destructive value was averaged for all voxels throughout the volume of the treated tumor. At each readpoint, the volumetric perfusion time was normalized to the value obtained at baseline (day 0).

Likewise, for volume experiments, the measured volume at each readpoint was normalized to the value obtained at day 0.

Significance between treated and untreated distributions was analyzed in Excel using a two-sided student's t-test with unequal variance. Significance between distributions were considered at a value of $p < 0.05$.

Results

Ultrasonic Molecular Imaging

PDX-R—Day 2 was the earliest readpoint at which there was a statistical difference between the untreated and treated populations when using USMI. On day 2, the mean volumetric targeted microbubble intensity in treated animals decreased by 51% from the baseline measurement at day 0 compared to an 20% increase in targeting for untreated animals (Untreated: 1.20±0.53 vs. Treated: 0.49±0.40; $p < 0.05$) (Figure 1A). On Day 7, the same trend was observed (Untreated: 0.70±0.31 vs. Treated: 0.08±0.09; $p < 0.05$), however, by day 14, there were no discernible differences between treated and untreated populations.

Volumetric ultrasound images of a representative treated and a representative untreated PDX-R at baseline and 48 hours after treatment are illustrated in Figure 2. Axial and lateral axes are displayed on each 3-D image to orient the reader to the plane of the ultrasound transducer. In addition, 2-D cross sections, as registered by these section axes, illustrate the level of targeting at each day for the treated and untreated animal. The green color overlay illustrates the microbubble adherence to $\alpha_v\beta_3$ where the brightness is assumed to be correlated with the degree of molecular marker expression.

PDX-NR—In the PDX-NR cohort, there were no significant differences between treated and untreated populations at any readpoint in the 14-day study (Figure 1B). For clarity, Table I provides the volumetric USMI data for both the PDX-R and PDX-NR cohorts at all readpoints.

Dynamic Contrast Enhanced - Perfusion Imaging

PDX-R—Day 14 was the earliest readpoint at which there was a statistical difference between the untreated and treated populations when using DCE-PI. Of note, by day 2 there was an increase in mean volumetric TT20 values relative to day 0. While there was not a significant difference between treated and untreated populations at this readpoint, there was an increasing difference between treated and untreated population until day 14. As will be shown in the following subsection, this trend was not observed in the PDX-NR cohort. On day 14, the mean volumetric TT20 value increased by 31% from baseline in treated animals compared to a 6% decrease in the TT20 for untreated animals (Untreated: 0.94±0.23 vs. Treated: 1.31±0.22; $p < 0.05$) (Figure 3A).

PDX-NR—There were no significant differences between treated and untreated populations at any readpoint with the PDX-NR cohort (Figure 3B). Table II provides the raw volumetric DCE-PI values for each group at each readpoint.

Volume Measurements

PDX-R—In the PDX-R cohort of animals, there was no statistical difference between treated and untreated populations when measuring the volume of the tumor at any readpoint (Figure 4). However, the difference in tumor volume between treated and untreated animals began to increase starting at day 7, as would be expected in this PDX-R, since it is characterized by known response to MLN8237 treatment. This trend was not observed in the PDX-NR cohort.

PDX-NR—As with the PDX-R group, there was no observed statistical difference between treated and untreated populations when measuring the volume of the tumor at any readpoint. Table III summarizes the volume data collected for the responder and non-responder groups.

Discussion and Conclusion

In this study, USMI of angiogenesis showed a statistical difference between treated and untreated PDX-R populations after 48 hours of treatment. In contrast, there was no significant difference between treated and untreated groups at the same readpoints in the PDX-NR cohort. Thus, our USMI study clearly illustrates the viability of the technique for monitoring the response to therapy and classifying and characterizing tumors as responders and non-responders in pre-clinical evaluations where comparison with a baseline untreated control is available. In addition, this imaging method used for monitoring biomarker expression was the earliest of the three tested techniques in detecting a change, as reflected by the time at which change was detected (48 hours) and the statistical significance between groups ($p = 0.03$) in the PDX-R cohort.

Data illustrate that the degree of $\alpha_v\beta_3$ expression decreased at a faster rate for treated animals as compared to untreated animals in the PDX-R group, which was the observed trend over a 7-day window (−12% vs. −5%). Likewise, the PDX-NR group also experienced this trend, though the treated group was not significantly different from the untreated group (−4% vs. −2%, $p = 0.08$). This data may suggest that the PDX-NR group partially responded to the therapy, which may explain why we were unable to differentiate between the treated responder group and the treated non-responder group without normalizing to the untreated control cohorts.

DCE-PI, which is a measurement of vascular perfusion and thus MVD, showed statistical significance on day 14 between treated and untreated populations in the PDX-R cohort. Thus, USMI provided information about therapy response prior to DCE-PI for the PDX-R group. This result was not unexpected, as changes in the microvasculature are likely preceded by a corresponding change in biomarker expression. Furthermore, it was predicted that healthy vasculature would have faster perfusion times relative to unhealthy microvasculature, which was the observed outcome in the DCE-PI study. (48, 49) Data illustrated that the perfusion times increased at a faster rate during treatment compared to untreated tumors, which was observed in our study (2% vs. 0%). Based on our results, DCE-PI appears to be a viable alternative to volume measurements in terms of classification and characterization of responder and non-responder cohorts for pre-clinical evaluations.

Using volume measurements for therapeutic pre-clinical mouse model studies is rapid, non-invasive and inexpensive; however, it is also high in variability, which is an impediment as a means for monitoring the response to therapy (50, 51). In this study, volume measurements obtained with ultrasound did not show any significant differences between treated and untreated groups on any day for either the PDX-R or PDX-NR cohorts. In contrast, USMI and DCE-PI both demonstrated their ability to detect changes between treated and untreated populations in the responder group at earlier time points than with volume measurements. As with the DCE-PI technique, the volume curves for the treated and untreated treatment populations of the PDX-NR cohort during the time period of the imaging study provided no evidence to support that there was a partial response to therapy.

There are a number of factors that could have impacted how the evaluated techniques performed in this study. For instance, the strength of the evaluated therapeutic may favor one method over the other in terms of the measured effect. The stronger the therapeutic, the more likely the method may detect a change at earlier time points. An increase in dose was not evaluated in this study. Secondly, the readpoint sampling may have contributed to the observed performance of the DCE-PI study. If imaging was performed more frequently between day 2 and day 14, then more observed days with a significant difference between populations might have been observed prior to day 14. The tumor type may also have contributed to the performance of each technique. In the pancreatic adenocarcinoma tumor model that was used in this study, necrosis was observed to increase throughout the length of the study. As a tumor becomes more necrotic, it also becomes less vascular, which ultimately makes the untreated groups look similar to the treated groups. For instance, the untreated populations (PDX-R group) in our USMI study showed a gradual decrease in $\alpha_v\beta_3$ expression. This decrease over time can mean one of two things. Either the vessels are not expressing the angiogenic biomarker or there is not a vessel there to express the biomarker, which is more likely given that areas of necrosis were also observed in the DCE-PI study. Thus, as the untreated tumor becomes more naturally necrotic over time, it confounds the ability of the technique to distinguish between the treated and untreated groups. In future studies, for both USMI and DCE-PI, each of these factors must be explored. Finally, significance of this study was limited due to its short-term observation period. Future work will need to include larger subject numbers and longer time scales to more thoroughly validate our preliminary observations.

In order to evaluate the sensitivity of each technique's ability to identify a responder over a non-responder in a clinical situation, we evaluated the significance between treated groups at each readpoint. None of the evaluated techniques showed a statistically significant difference between treated groups (PDX-R treated vs. PDX-NR treated) at any readpoint. Our study indicated that normalization relative to the untreated groups needed to be performed to illustrate the significance of the data. Since normalization would not be relevant in a clinical situation, the methods as described here would not be clinically translatable without further improvement. Nevertheless, USMI and DCE-PI have illustrated substantial potential in pre-clinical response to therapy studies. Furthermore, it is very possible that these techniques still may be clinically significant without normalization in different tumor models or with different therapeutic approaches, or after further improvements in imaging and contrast agent technology.

In conclusion, we showed that we could successfully classify a tumor as a responder or a non-responder with both USMI (day 2 & day 7) and DCE-PI (day 14) and at earlier time points than with volume measurements (~4 weeks). Second, we were able to characterize how the PDX-R and PDX-NR groups would respond over a 14-day period, which is an essential component in understanding the pathophysiologic mechanisms of a particular type of cancer and it is an evolutionary step for a clinical-type application. Based on our results, we feel that classification and characterization of a tumor in pre-clinical evaluations using USMI may allow for more effective drug development and an improvement in pharmacodynamic monitoring through reduced cycle times. Finally, since a volumetric approach has been shown to provide more accurate data than an equivalent 2-D analysis, we have succeeded in illustrating the strengths of 3-D USMI and 3-D DCE-PI for characterizing a tumor's response to therapy in pre-clinical studies.

Acknowledgements

Funding was provided by funds from the UNC Lineberger Cancer Center as well as NIH R01 EB009066 (PD), R01-CA140424-01 –A1 (JJY), and American Cancer Society 118777-PF-10-023-01-CSM (NFN). The authors would also like to acknowledge the assistance of James Tsuruta in cRGD/cRAD lipid conjugation that was used for targeted microbubble fabrication. The authors would also like to thank Charlene Ross and the Animal Studies Core Facility for their excellent technical assistance throughout this study. Finally, the authors would like to acknowledge the assistance of Ismayil Guracar from Siemens Medical Solutions in the development of the motion-corrected perfusion imaging algorithms that were utilized in this work.

References

1. Fu J, Bian M, Jiang Q, Zhang C. Roles of aurora kinases in mitosis and tumorigenesis. Mol Cancer Res. 2007; 5(1):1–10. [PubMed: 17259342]
2. Glover DM, Leibowitz MH, McLean DA, Parry H. Mutations in aurora prevent centrosome separation leading to the formation of monopolar spindles. Cell. 1995; 81(1):95–105. [PubMed: 7720077]
3. Hirota T, Kunitoku N, Sasayama T, Marumoto T, Zhang D, Nitta M, Hatakeyama K, Saya H. Aurora-a and an interacting activator, the lim protein ajuba, are required for mitotic commitment in human cells. Cell. 2003; 114(5):585–598. [PubMed: 13678582]
4. Li D, Zhu J, Firozi PF, Abbruzzese JL, Evans DB, Cleary K, Friess H, Sen S. Overexpression of oncogenic stk15/btak/aurora a kinase in human pancreatic cancer. Clin Cancer Res. 2003; 9(3):991–997. [PubMed: 12631597]
5. Tatsuka M, Katayama H, Ota T, Tanaka T, Odashima S, Suzuki F, Terada Y. Multinuclearity and increased ploidy caused by overexpression of the aurora- and ipl1-like midbody-associated protein mitotic kinase in human cancer cells. Cancer Res. 1998; 58(21):4811–4816. [PubMed: 9809983]
6. Zhou H, Kuang J, Zhong L, Kuo WL, Gray JW, Sahin A, Brinkley BR, Sen S. Tumour amplified kinase stk15/btak induces centrosome amplification, aneuploidy and transformation. Nat Genet. 1998; 20(2):189–193. [PubMed: 9771714]
7. Katayama H, Ota T, Jisaki F, Ueda Y, Tanaka T, Odashima S, Suzuki F, Terada Y, Tatsuka M. Mitotic kinase expression and colorectal cancer progression. J Natl Cancer Inst. 1999; 91(13):1160–1162. [PubMed: 10393726]
8. Gautschi O, Heighway J, Mack PC, Purnell PR, Lara PN, Gandara DR. Aurora kinases as anticancer drug targets. Clin Cancer Res. 2008; 14(6):1639–1648. [PubMed: 18347165]
9. Kovar H. Aurka inhibitors: right in time. Pediatr Blood Cancer. 2010; 55(1):3–4. [PubMed: 20486161]
10. Michalski MH, Chen X. Molecular imaging in cancer treatment. Eur J Nucl Med Mol Imaging. 2011; 38(2):358–377. [PubMed: 20661557]

11. Van den Abbeele AD, Gatsonis C, de Vries DJ, Melenevsky Y, Szot-Barnes A, Yap JT, Godwin AK, Rink L, Huang M, Blevins M, Sicks J, Eisenberg B, Siegel BA. ACRIN 6665/RTOG 0132 Phase II Trial of Neoadjuvant Imatinib Mesylate for Operable Malignant Gastrointestinal Stromal Tumor: Monitoring with 18F-FDG PET and Correlation with Genotype and GLUT4 Expression. J Nucl Med. 2012; 53(4):567–574. [PubMed: 22381410]
12. Prior JO, Montemurro M, Orcurto MV, Michielin O, Luthi F, Benhattar J, Guillou L, Elsig V, Stupp R, Delaloye AB, Leyvraz S. Early Prediction of Response to Sunitinib After Imatinib Failure by 18F-Fluorodeoxyglucose Positron Emission Tomography in Patients With Gastrointestinal Stromal Tumor. J Clin Oncol. 2009; 27(3):439–445. [PubMed: 19064982]
13. Lanza GM, Wickline S. Targeted ultrasonic contrast agents for molecular imaging and therapy. Curr Probl Cardiol. 2003; 28(12):625–653. [PubMed: 14691443]
14. Lindner JR, Dayton PA, Coggins MP, Ley KF, Song J, Ferrara KW, Kaul S. Noninvasive imaging of inflammation by ultrasound detection of phagocytosed microbubbles. Circulation. 2000; 102(5): 531–538. [PubMed: 10920065]
15. Lindner JR. Molecular imaging of cardiovascular disease with contrast-enhanced ultrasonography. Nat Rev Cardiol. 2009; 6(7):475–481. [PubMed: 19506587]
16. Dayton PA, Ferrara KW. Targeted imaging using ultrasound. J Magn Reson Imaging. 2002; 16(4): 362–377. [PubMed: 12353252]
17. Lindner JR, Coggins MP, Kaul S, Klibanov AL, Brandenburger GH, Ley KF. Microbubble persistence in the microcirculation during ischemia/reperfusion and inflammation is caused by integrin- and complement-mediated adherence to activated leukocytes. Circulation. 2000; 101(6): 668–675. [PubMed: 10673260]
18. Villanueva FS, Lu E, Bowry S, Kilic S, Tom EM, Wang J, Gretton J, Pacella JJ, Wagner WR. Myocardial ischemic memory imaging with molecular echocardiography. Circulation. 2007; 115(3):345–352. [PubMed: 17210843]
19. Villanueva FS, Jankowski RJ, Klibanov S, Pina ML, Alber SM, Watkins SC, Brandenburger GH, Wagner WR. Microbubbles targeted to intercellular adhesion molecule-1 bind to activated coronary artery endothelial cells. Circulation. 1998; 98(1):1–5. [PubMed: 9665051]
20. Weinberg, R. Garland Science. New York: Taylor and Francis Group, LLC; 2007. The biology of cancer.
21. Kim D, Chung J. Akt: versatile mediator of cell survival and beyond. J Biochem Mol Biol. 2002; 35(1):106–115. [PubMed: 16248975]
22. Lin YH, Lee CC, Chan WL, Chang WH, Wu YC, Chang JG. 16-hydroxycleroda-3,13-dien-15,16-olide deregulates pi3k and aurora b activities that involve in cancer cell apoptosis. Toxicology. 2011; 285(1–2):72–80. [PubMed: 21530604]
23. Leong-Poi H, Christiansen JP, Klibanov AL, Kaul S, Lindner JR. Noninvasive assessment of angiogenesis by ultrasound and microbubbles targeted to alpha(v)-integrins. Circulation. 2003; 107(3):455–460. [PubMed: 12551871]
24. Schumann PA, Christiansen JP, Quigley RM, McCreery TP, Sweitzer RH, Unger EC, Lindner JR, Matsunaga TO. Targeted-microbubble binding selectively to gpiib iiia receptors of platelet thrombi. Invest Radiol. 2002; 37(11):587–593. [PubMed: 12393970]
25. Willmann JK, Kimura RH, Deshpande N, Lutz AM, Cochran JR, Gambhir SS. Targeted contrast-enhanced ultrasound imaging of tumor angiogenesis with contrast microbubbles conjugated to integrin-binding knottin peptides. J Nucl Med. 2010; 51(3):433–440. [PubMed: 20150258]
26. Willmann JK, Paulmurugan R, Chen K, Gheysens O, Rodriguez-Porcel M, Lutz AM, Chen IY, Chen X, Gambhir SS. Us imaging of tumor angiogenesis with microbubbles targeted to vascular endothelial growth factor receptor type 2 in mice. Radiology. 2008; 246(2):508–518. [PubMed: 18180339]
27. Weller GER, Lu E, Csikari MM, Klibanov AL, Fischer D, Wagner WR, Villanueva FS. Ultrasound imaging of acute cardiac transplant rejection with microbubbles targeted to intercellular adhesion molecule-1. Circulation. 2003; 108(2):218–224. [PubMed: 12835214]
28. Streeter JE, Gessner RC, Tsuruta J, Feingold S, Dayton PA. Assessment of molecular imaging of angiogenesis with three-dimensional ultrasonography. Mol Imaging. 2011; 10(6):460–468. [PubMed: 22201537]

29. Streeter JE, Gessner RC, Miles I, Dayton PA. Improving sensitivity in ultrasound molecular imaging by tailoring contrast agent size distribution: in vivo studies. Mol Imaging. 2010; 9(2):87–95. [PubMed: 20236606]
30. Pochon S, Tardy I, Bussat P, Bettinger T, Brochot J, von Wronski M, Passantino L, Schneider M. Br55: a lipopeptide-based vegfr2-targeted ultrasound contrast agent for molecular imaging of angiogenesis. Invest Radiol. 2010; 45(2):89–95. [PubMed: 20027118]
31. Palmowski M, Huppert J, Ladewig G, Hauff P, Reinhardt M, Mueller MM, Woenne EC, Jenne JW, Maurer M, Kauffmann GW, Semmler W, Kiessling F. Molecular profiling of angiogenesis with targeted ultrasound imaging: early assessment of antiangiogenic therapy effects. Mol Cancer Ther. 2008; 7(1):101–109. [PubMed: 18202013]
32. Wei K, Jayaweera AR, Firoozan S, Linka A, Skyba DM, Kaul S. Quantification of myocardial blood flow with ultrasound-induced destruction of microbubbles administered as a constant venous infusion. Circulation. 1998; 97(5):473–483. [PubMed: 9490243]
33. Pollard RE, Sadlowski AR, Bloch SH, Murray L, Wisner ER, Griffey S, Ferrara KW. Contrast-assisted destruction-replenishment ultrasound for the assessment of tumor microvasculature in a rat model. Technol Cancer Res Treat. 2002; 1(6):459–470. [PubMed: 12625773]
34. Pollard RE, Dayton PA, Watson KD, Hu X, Guracar IM, Ferrara KW. Motion corrected cadence cps ultrasound for quantifying response to vasoactive drugs in a rat kidney model. Urology. 2009; 74(3):675–681. [PubMed: 19589583]
35. Stieger SM, Bloch SH, Foreman O, Wisner ER, Ferrara KW, Dayton PA. Ultrasound assessment of angiogenesis in a matrigel model in rats. Ultrasound Med Biol. 2006; 32(5):673–681. [PubMed: 16677927]
36. Du J, Li FH, Fang H, Xia J-G, Zhu C-X. Correlation of real-time gray scale contrast-enhanced ultrasonography with microvessel density and vascular endothelial growth factor expression for assessment of angiogenesis in breast lesions. J Ultrasound Med. 2008; 27(6):821–831. [PubMed: 18499842]
37. Foote RL, Weidner N, Harris J, Hammond E, Lewis JE, Vuong T, Ang KK, Fu KK. Evaluation of tumor angiogenesis measured with microvessel density (mvd) as a prognostic indicator in nasopharyngeal carcinoma: results of rtog 9505. Int J Radiat Oncol Biol Phys. 2005; 61(3):745–753. [PubMed: 15708253]
38. El-Assal ON, Yamanoi A, Soda Y, Yamaguchi M, Igarashi M, Yamamoto A, Nabika T, Nagasue N. Clinical significance of microvessel density and vascular endothelial growth factor expression in hepatocellular carcinoma and surrounding liver: possible involvement of vascular endothelial growth factor in the angiogenesis of cirrhotic liver. Hepatology. 1998; 27(6):1554–1562. [PubMed: 9620326]
39. Sirsi SR, Flexman ML, Vlachos F, Huang J, Hernandez SL, Kim HK, Johung TB, Gander JW, Reichstein AR, Lampl BS, Wang A, Hielscher AH, Kandel JJ, Yamashiro DJ, Borden MA. Contrast ultrasound imaging for identification of early responder tumor models to anti-angiogenic therapy. Ultrasound Med Biol. 2012; 38(6):1019–1029. [PubMed: 22425376]
40. Feingold S, Gessner RC, Guracar IM, Dayton PA. Quantitative volumetric perfusion mapping of the microvasculature using contrast ultrasound. Invest Radiol. 2010; 45(10):669–674. [PubMed: 20808232]
41. Hoyt K, Sorace A, Saini R. Quantitative Mapping of Tumor Vascularity Using Volumetric Contrast-Enhanced Ultrasound. Invest Radiol. 2012; 47(3):167–174. [PubMed: 22104962]
42. Rubio-Viqueira B, Jimeno A, Cusatis G, Zhang X, Iacobuzio-Donahue C, Karikari C, Shi S, Danenberg K, Danenberg PV, Kuramochi H, Tanaka K, Singh S, Salimi-Moosavi H, Bouraoud N, Amador ML, Altiok S, Kulesza P, Yeo C, Messersmith W, Eshleman J, Hruban RH, Maitra A, Hidalgo M. An In vivo Platform for Translational Drug Development in Pancreatic Cancer. Clin Cancer Res. 2006; 12(15):4652–4661. [PubMed: 16899615]
43. Decaudin D. Primary human tumor xenografted models (’tumorgrafts’) for good management of patients with cancer. Anticancer drugs. 2011; 22(9):827–841. [PubMed: 21623183]
44. Ruoslahti E. Integrins as signaling molecules and targets for tumor therapy. Kidney Int. 1997; 51(5):1413–1417. [PubMed: 9150452]

45. Sirsi S, Feshitan JA, Kwan J, Homma S, Borden MA. Effect of microbubble size on fundamental mode high frequency ultrasound imaging in mice. Ultrasound Med Biol. 2010; 36(6):935–948. [PubMed: 20447755]

46. Feshitan JA, Chen CC, Kwan JJ, Borden MA. Microbubble size isolation by differential centrifugation. J Colloid Interface Sci. 2009; 329(2):316–324. [PubMed: 18950786]

47. Stieger SM, Dayton PA, Borden MA, Caskey CF, Griffey SM, Wisner ER, Ferrara KW. Imaging of angiogenesis using cadence contrast pulse sequencing and targeted contrast agents. Contrast Media Mol Imaging. 2008; 3(1):9–18. [PubMed: 18335479]

48. Guibal A, Taillade L, Mule S, Comperat E, Badachi Y, Golmard JL, Guillou-Buffello D, Rixe O, Bridal SL, Lucidarme O. Noninvasive contrast-enhanced US quantitative assessment of tumor microcirculation in a murine model: effect of discontinuing anti-VEGF therapy. Radiology. 2010; 254(2):420–429. [PubMed: 20093514]

49. Zhou J, Cao L, Liu J, Zheng W, Liu M, Luo R, Han F, Li A. Quantitative Assessment of Tumor Blood Flow in Mice after Treatment with Different Doses of an Antiangiogenic Agent with Contrast-enhanced Destruction-Replenishment US. Radiology. 2011; 259(2):406–413. [PubMed: 21292869]

50. Ayers GD, McKinley ET, Zhao P, Fritz JM, Metry RE, Deal BC, Adlerz KM, Coffey RJ, Manning HC. Volume of preclinical xenograft tumors is more accurately assessed by ultrasound imaging than manual caliper measurements. J Ultrasound Med. 2010; 29(6):891–901. [PubMed: 20498463]

51. Euhus DM, Hudd C, LaRegina MC, Johnson FE. Tumor measurement in the nude mouse. J Surg Oncol. 1986; 31(4):229–234. [PubMed: 3724177]

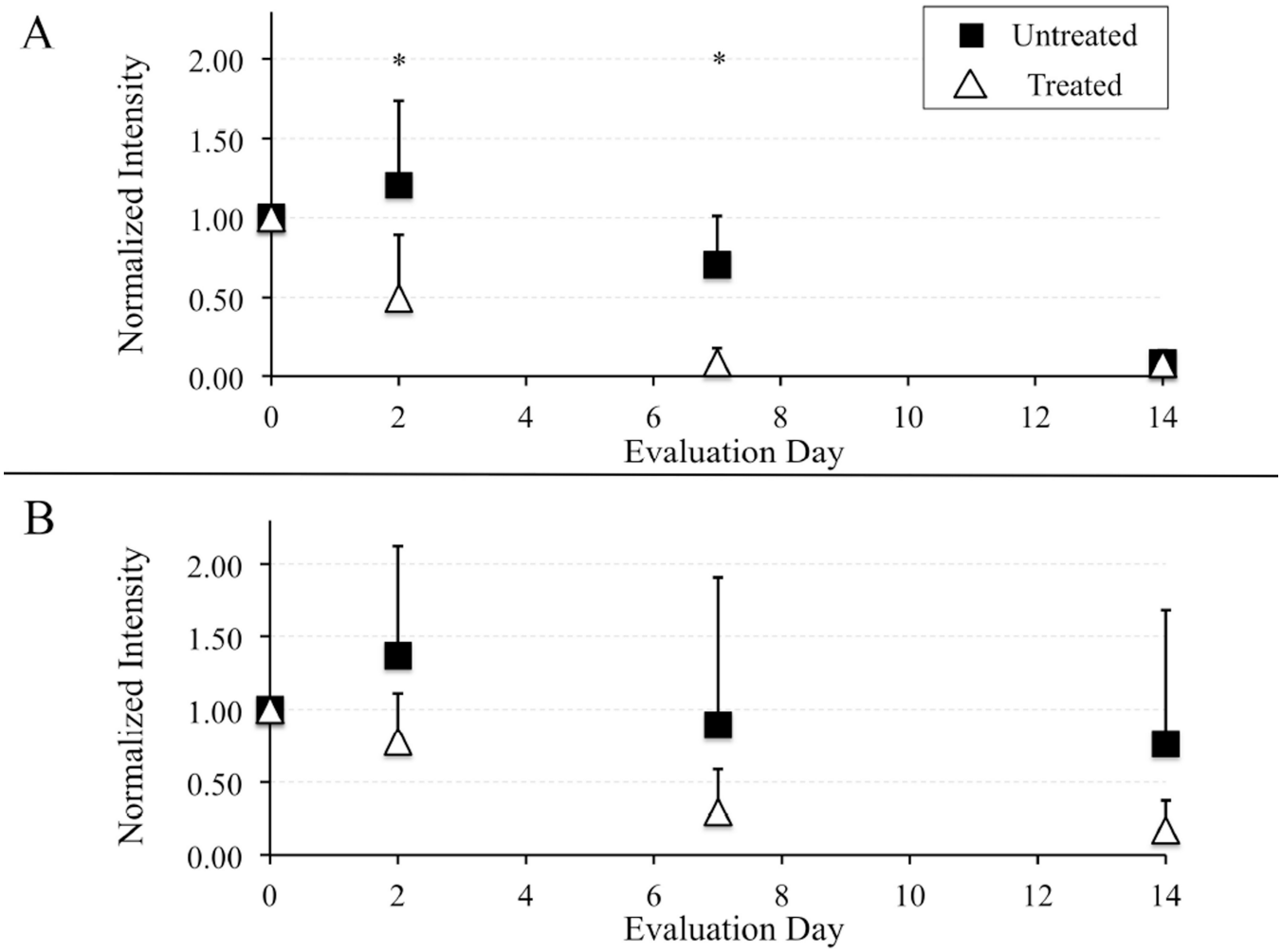

Figure 1.

A) The percent change in volumetric targeted microbubble intensity for treated and untreated animals before and after therapy in a tumor type that responds to MLN8237 (N=7). B) The percent change in volumetric targeted microbubble intensity for treated and untreated animals before and after therapy in a tumor that does not respond to MLN8237 (N=7). * $p < 0.05$ for treated group relative to untreated group.

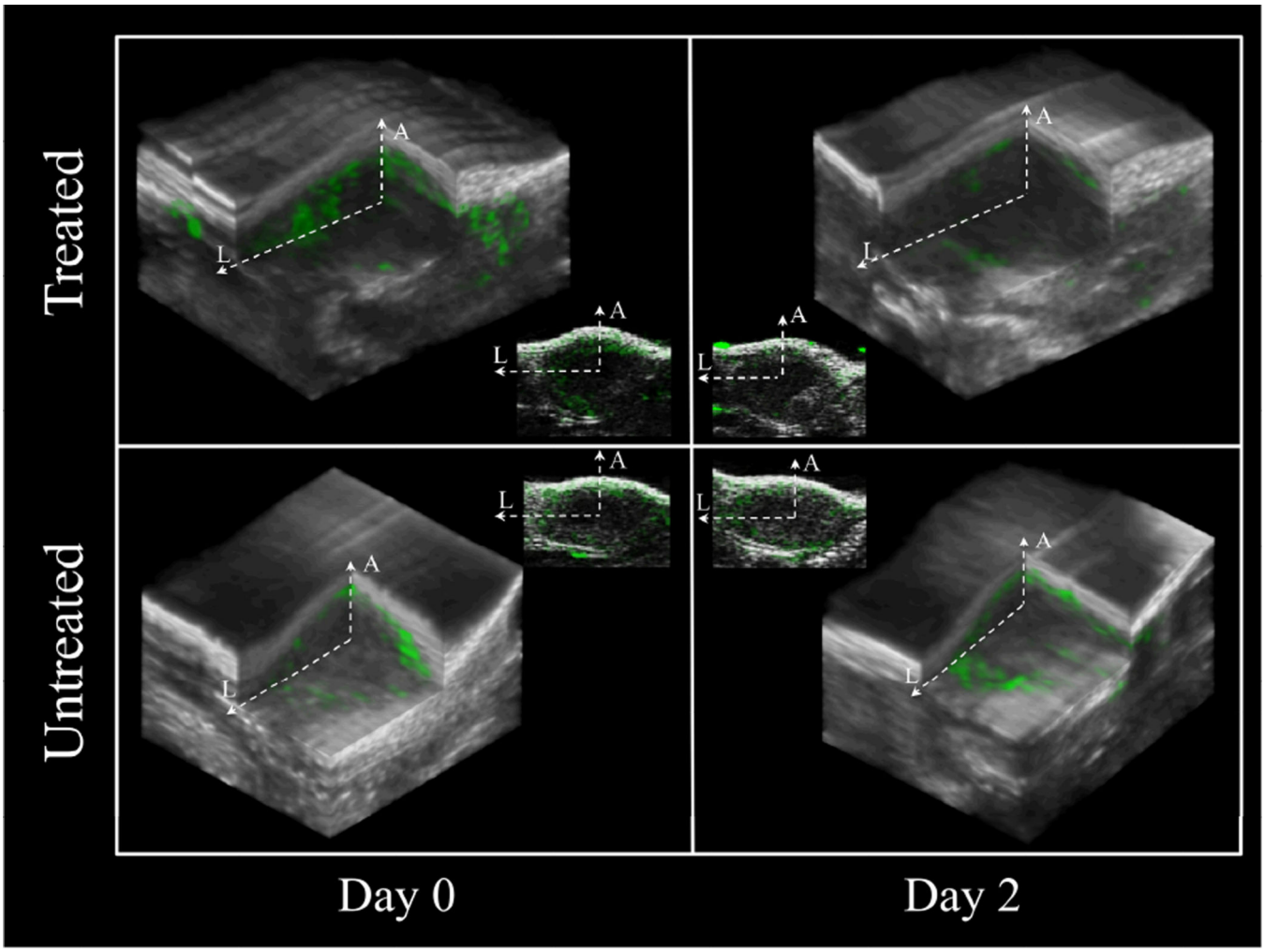

Figure 2.

3-D ultrasound images of a representative treated and a representative untreated tumor (PDX-R). A (axial) and L (lateral) axes are displayed to orient the reader to the traditional ultrasound b-mode image plane. 2-D cross sections as registered by these section axes are displayed in the central region of each panel. The green color overlay illustrates the microbubble adherence to $\alpha_v\beta_3$, an angiogenic biomarker. The brightness of the green image overlay is assumed to be correlated with the degree of molecular marker expression.

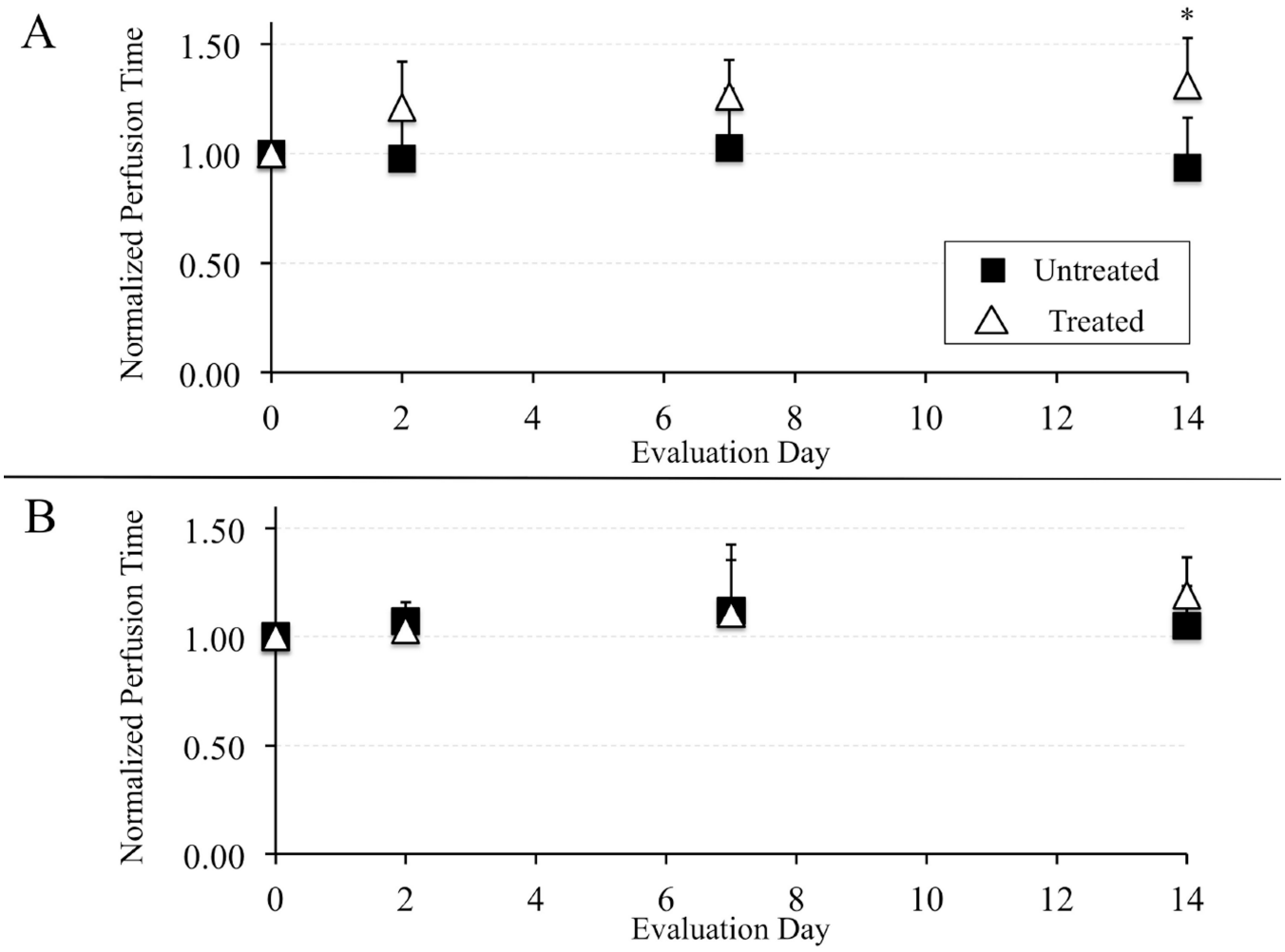

Figure 3.

A) The average volumetric perfusion times before and after therapy for treated and untreated animals in a tumor type that responds to MLN8237 (N=7). B) The average volumetric perfusion times before and after therapy for treated and untreated animals in a tumor type that does not respond to MLN8237 (N=7). * $p < 0.05$ for treated group as compared to untreated group.

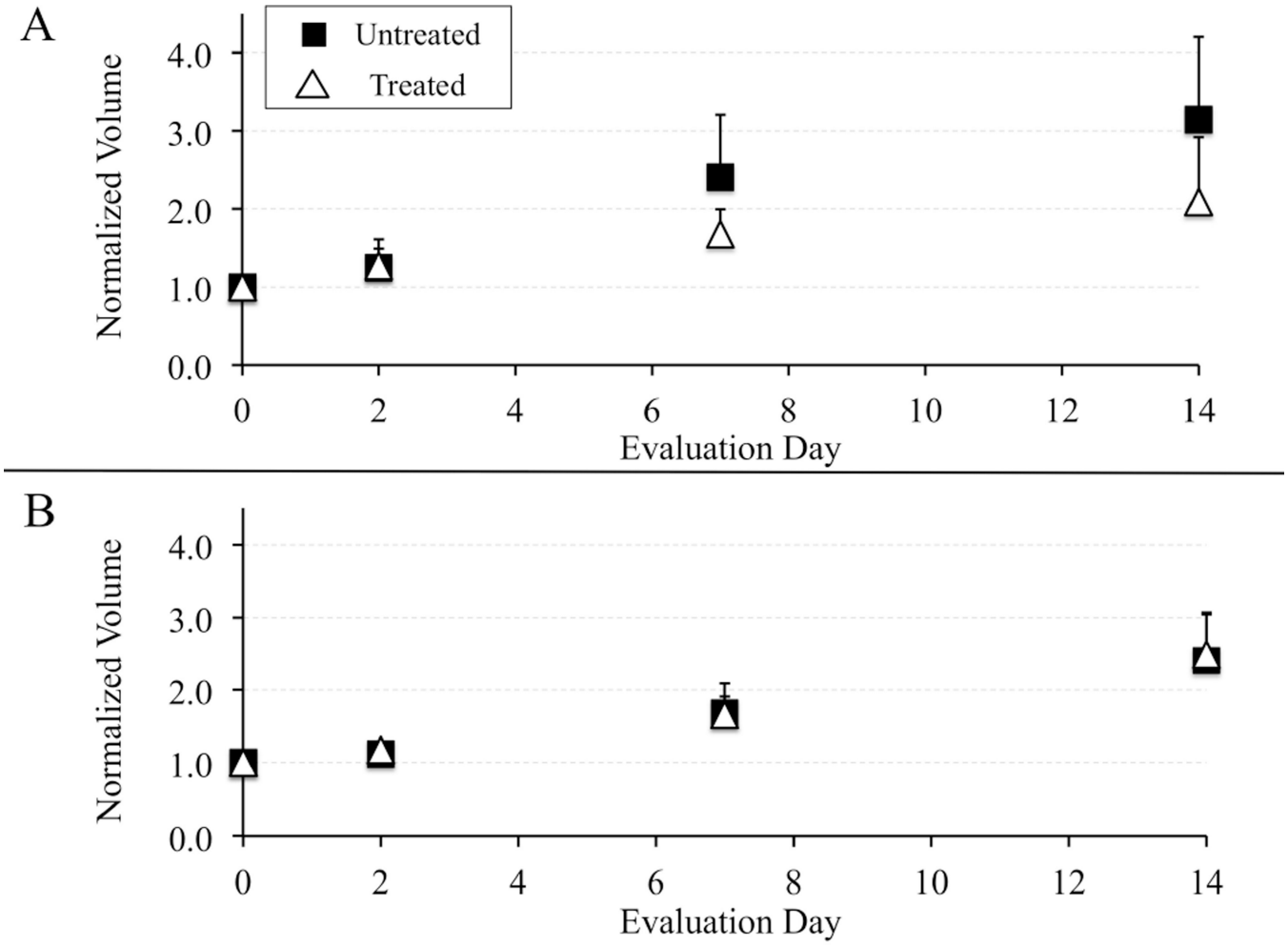

Figure 4.

A) The tumor volume as measured by regions of interest from ultrasound b-mode for treated and untreated animals in a tumor known to respond to MLN8237 (N=7). B) The tumor volume as measured by regions of interest from ultrasound b-mode for treated and untreated animals in a tumor known not to respond to MLN8237 (N=7).

Table I

Summary of the normalized volumetric USMI data for both treated and untreated animals in the PDX-R and PDX-NR cohorts. This data is supplementary to the plots in Figure 1.

		USMI			
		Day 0	**Day 2**	**Day 7**	**Day 14**
PDX-R	Treated	1.00 ± 0.0	0.49 ± 0.4	0.08 ± 0.1	0.08 ± 0.1
	Untreated	1.00 ± 0.0	1.20 ± 0.5	0.70 ± 0.3	0.08 ± 0.1
	p		0.03	0.01	1.00
PDX-NR	Treated	1.00 ± 0.0	0.77 ± 0.3	0.30 ± 0.3	0.17 ± 0.2
	Untreated	1.00 ± 0.0	1.37 ± 0.8	0.89 ± 1.0	0.76 ± 0.9
	p		0.08	0.16	0.15

Table II

Summary of the normalized volumetric DCE-PI data for both treated and untreated animals in the PDX-R and PDX-NR cohorts. This data corresponds to the plots in Figure 3.

		DCE-PI			
		Day 0	**Day 2**	**Day 7**	**Day 14**
PDX-R	Treated	1.00 ± 0.0	1.21 ± 0.2	1.26 ± 0.2	1.31 ± 0.2
	Untreated	1.00 ± 0.0	0.98 ± 0.2	1.02 ± 0.3	0.94 ± 0.2
	p		0.07	0.19	0.04
PDX-NR	Treated	1.00 ± 0.0	1.03 ± 0.1	1.11 ± 0.3	1.19 ± 0.2
	Untreated	1.00 ± 0.0	1.07 ± 0.1	1.12 ± 0.2	1.05 ± 0.2
	p		0.52	0.93	0.22

Table III

Summary of the normalized volumetric data for both treated and untreated animals in the PDX-R and PDX-NR cohorts. This data corresponds to the plots in Figure 5.

		Volume			
		Day 0	**Day 2**	**Day 7**	**Day 14**
PDX-R	Treated	1.00 ± 0.0	1.27 ± 0.2	1.68 ± 0.3	2.09 ± 0.8
	Untreated	1.00 ± 0.0	1.24 ± 0.4	2.41 ± 0.8	3.14 ± 1.1
	p		0.88	0.09	0.12
PDX-NR	Treated	1.00 ± 0.0	1.17 ± 0.1	1.66 ± 0.3	2.50 ± 0.6
	Untreated	1.00 ± 0.0	1.12 ± 0.1	1.68 ± 0.4	2.40 ± 0.7
	p		0.39	0.91	0.80